Nanoscale Advances

Accepted Manuscript

This article can be cited before page numbers have been issued, to do this please use: Md. S. Rana, A. Rahim, Md. R. Hasan, M. Shahinuzzaman, A. N. Ahmed, Md. S. Quddus, C. K. Roy, M. Hossain and M. Shah Jamal, *Nanoscale Adv.*, 2026, DOI: 10.1039/D5NA00957J.

ROYAL SOCIETY OF CHEMISTRY

rsc.li/nanoscale-advances

View Article Online
DOI: 10.1039/D5NA00957J

Tailoring the structural and morphological properties of $LiNi_{0.5}Co_{0.2}Mn_{0.3}O_2$ cathode material via a novel mixed-solvothermal method

Md. Sohel Rana[1], Abdur Rahim[1], Rakibul Hasan[1], M. Shahinuzzaman[1], Aninda Nafis Ahmed[2], Md. Saiful Quddus[3], Chanchal Kumar Roy[4], Mosharof Hossain[1], Mohammad Shah Jamal[1,*]

[1] *Institute of Energy Research and Development (IERD), Bangladesh Council of Scientific and Industrial Research (BCSIR), Dr. Qudrat-E-Khuda Road, Dhanmondi, Dhaka-1205, Bangladesh.*

[2] *Pilot Plant and Process Development Centre (PP&PDC), Research and Development (IERD), Bangladesh Council of Scientific and Industrial Research (BCSIR), Dr. Qudrat-E-Khuda Road, Dhanmondi, Dhaka-1205, Bangladesh.*

[3] *Institute of Glass and Ceramic Research and Testing (IGCRT), Bangladesh Council of Scientific and Industrial Research (BCSIR), Dr. Qudrat-E-Khuda Road, Dhanmondi, Dhaka 1205, Bangladesh.*

[4] *Department of Chemistry, Bangladesh University of Engineering and Technology, Dhaka 1000, Bangladesh.*

Corresponding author: msjamal@bcsir.gov.bd (MSJ)

View Article Online
DOI: 10.1039/D5NA00957J

Abstract

$LiNi_{0.5}Co_{0.2}Mn_{0.3}O_2$ (NCM523) is a promising cathode material for lithium-ion battery with high capacity, stability, and environmental benefits, but conventional synthesis methods often cause structural degradation and cation mixing that hinder performance. In this study, a novel, optimized, and facile mixed-solvothermal approach mediated by ethylene glycol, water, and ethanolamine was employed to synthesize NCM523 cathode materials with enhanced crystallinity and optimized morphology. The effects of different calcination temperatures (700 °C, 800 °C, and 900 °C) on the structural, morphological, and chemical properties were systematically investigated. X-ray diffraction (XRD) analysis confirmed the formation of a well-ordered layered structure, with the sample mediated in ethylene glycol, water & ethanolamine and calcined at 800 °C (NCM-800), exhibiting superior phase purity and minimal cation disorder. The sample calcined at 800 °C exhibited the highest crystallite size of 37 nm and an intensity ratio of 1.42 in the case of (003) plane to (104), which indicates the lowest cation mixing of Li^+/Ni^{2+} ions. X-ray photoelectron spectroscopy (XPS) further revealed optimal Ni^{2+}/Ni^{3+} ratios (0.23) and lattice oxygen retention in NCM-800, indicating robust redox activity and minimal oxygen vacancies. Field emission scanning electron microscopy (FE-SEM) demonstrated that NCM-800 possessed uniform, densely packed spherical particles with minimal surface defects, contributing to improved mechanical integrity and electrochemical stability. Compared to samples calcined at lower or higher temperatures, NCM-800 achieved an optimal balance between crystallinity, particle morphology, and structural robustness. These findings highlight the potential of the mixed-solvothermal method as a promising, scalable, and cost-effective strategy for the synthesis of high-performance NCM523 cathode materials, paving the way for their application in next-generation lithium-ion batteries and advanced energy storage systems.

Keywords

Cathodic material, Mixed solvothermal method, Energy storage, Calcination temperature, Li-ion batteries,

View Article Online
DOI: 10.1039/D5NA00957J

Introduction

The growing demand for electric cars, hybrid electric vehicles (HEVs), portable electronics, and the substantial conversion from fossil fuels to renewable energy sources such as solar, hydropower, geothermal, biofuels, and wind power are central to addressing global climate transformation and dropping greenhouse gas emissions [1,2]. However, one of the critical challenges related to the intermittent nature of renewable energy generation is that it causes energy production to be inconsistent due to fluctuating weather patterns. This highlights the importance of developing efficient energy storage systems that can store excess energy during ultimate production and release it when consumption is high or generation is low, thereby driving the demand for advanced energy storage technologies. Lithium-ion batteries (LIBs) are now the most promising options among the many energy sources because of their high discharge-specific capability, large energy density, extended cycle life, affordability, environmental generosity, relatively lightweight design, and scalability from small devices to large industrial applications [3–5]. Powering everything from laptops and smartphones to electric vehicles and grid-based power storage devices, LIBs are now the cornerstone of contemporary energy storage systems. The performance of these batteries must be improved immediately due to the growing interest for sustainable and clean power sources, especially in the areas of energy density, high performance, safety, and affordability. However, there are still several obstacles to their widespread applications, which call for continued research and development to enhance the basic characteristics of LIBs, particularly in terms of their cathode materials, which are the main active materials of LIBs.

In the past decades, significant progress has been made in the development of cathode materials, with many promising candidates emerging, such as lithium cobalt oxide and phosphate ($LiCoO_2$ and $LiCoPO_4$) [6,7], lithium nickel oxide and phosphate ($LiNiO_2$ and $LiNiPO_4$) [8,9], lithium manganese oxide and phosphate ($LiMnO_2$ and $LiMnPO_4$)[10,11], lithium iron phosphate ($LiFePO_4$)[12]. These materials have been used extensively

View Article Online
DOI: 10.1039/D5NA00957J

in commercial batteries because of their stable cycling behavior, high discharge plateau, and moderate energy density and thermal stability. However, because of its high cost, unavailability to be use in high energy density applications, limited supply of cobalt, and mining-related environmental issues have led the researchers are looking into more affordable and environmentally friendly alternatives. $LiNi_{1-x-y}Co_xMn_yO_2$ (NCM) composites, which have a complex hexagonal R-3m and monoclinic C2/m structure, have recently drawn a lot of attention due to their higher reversible capacity (>200 mAh g^{-1}), high operating voltage, lower cost, and environmental friendliness by lowering their dependency on cobalt [13]. Among of them, the $LiNi_{0.5}Co_{0.2}Mn_{0.3}O_2$ (NCM523) has emerged as one of the most promising cathode materials for LIBs because of its notable tolerance to overcharge and discharge, good cycling behavior, reasonable thermal and structural stability, high-rate capability, and relatively high capacity with one leading plateau at about 4.7 V [14]. Despite these fascinating advantages, the NCM523 cathode material invariably exhibits irreversible structural rearrangement, undesired phase transition, and structural degradation during charge/discharge cycles leads to lattice distortion, cation mixing between Li^+ and Ni^{2+} ions, volume change, formation of oxygen vacancy, micro-cracks, and loss of lithium ions, all of which have a substantial impact on the electrochemical performance and, consequently, commercialization of electrochemical energy storage on a massive scale [15]. It is widely acknowledged that the construction, interface stability and cathode material electrochemical effectiveness are significantly influenced by the precursors and conditions of preparation. Based on the aforementioned query, the main strategies to minimize these drawbacks by improving structure and interface stability, experimental endeavors such as surface modification [16], heteroatom substitution by ion doping [17], morphology design [8], coating modification [7], and microwave-assisted synthesis [18] are widely used. Several synthesis methods, including the sol-gel method, solution combustion method [19], solid-state reaction [9], spray drying [10], hydrothermal method [7], co-precipitation method [16], and solvothermal method have been used to ensure optimized morphology, which enhances the electrochemical efficiency of the NCM523 cathode materials. The

View Article Online
DOI: 10.1039/D5NA00957J

hydrothermal/solvothermal method is the most promising strategy for researchers to develop nano and sub-micron cathode materials since it offers comparatively simple and trustworthy reaction conditions by using simple equipment. The opportunity to produce high-purity, uniform, and well-structured NCM523 cathode materials with better control over particle size, shape, and stoichiometry triggers the mixed solvothermal process individually [20]. It offers an assortment of benefits over alternative synthesis techniques, particularly in terms of electrochemical performance, scalability, and cost-effectiveness, making it a desirable option for advanced battery materials. The structural and electrochemical performance of layered NCM523 cathode materials is strongly influenced by synthesis conditions, particularly the choice of solvent in the solvothermal method. Solvents not only act as dispersing media but also control precursor chemistry, nucleation kinetics, and subsequent crystallization behavior [21]. Metal salt dissolution and complexation, as well as the crystallization process, are greatly influenced by the mixture of water and organic solvents like ethylene glycol (EG), polyethylene glycol (PEG), glycerol, ethanolamine (EA), triethylamine, and ethanol. Among the commonly employed solvents, EG has been widely used due to its high boiling point, viscosity, and ability to act as a polyol reducing agent. In NCM523 and related layered oxides, EG assisted synthesis has been reported to promote uniform precursor formation, enhance the lattice parameter ratio, and reduce cation disorder, thereby improving structural stability and electrochemical capacity [22]. However, the limited hydrolysis ability of EG often leads to incomplete decomposition of metal salts, uncontrolled nucleation, and smaller crystallite sizes, which may result in structural defects and inferior electrochemical performance. To overcome these shortcomings, mixed solvent systems have been explored. The incorporation of water into EG accelerates the hydrolysis of metal precursors, increases ionic mobility, improves reaction homogeneity, and promotes higher crystallinity compared with using EG alone [23]. Beyond binary solvents, the addition of organic amines, particularly EA, has shown further promise in controlling precursor chemistry. Conventional two-component mixes like EG/H_2O cannot match the synergistic chemical environment provided by the three-

View Article Online
DOI: 10.1039/D5NA00957J

component EG/H_2O/EA system. Unbalanced metal-ion precipitation and wide particle-size distributions result from weak coordination, even though EG/H_2O systems offer moderate hydrolysis control. The current system simultaneously balances hydrolysis kinetics, chelation strength, and sol-gel network formation by combining EG, water, and EA. This results in uniform nucleation and synchronized co-precipitation of Ni, Co, and Mn ions, which is not possible in binary systems. EG stabilizes polymeric chains, enhances dispersion, and stops particle overgrowth, water guarantees full but moderated hydrolysis, and ethanolamine offers regulated metal-ligand coordination and pH buffering. In the end, NCM523 cathode materials with improved phase purity, cation homogeneity, and electrochemical performance are produced by a precisely adjusted medium that encourages homogeneous precursor synthesis, narrow particle-size distributions, and cleaner thermal decomposition. It also acts as a pH-controlling agent, thereby regulating hydrolysis and condensation processes during agglomeration, and slows down nucleation and facilitates controlled crystal growth, which reduces cation mixing and enhances layered ordering and crystallinity [24]. The specific ratio of solvents affects the final morphology, determining whether the particles will form as spheres, rods, or plates, with organic solvents typically encouraging smoother particle growth and more controlled morphology. Additionally, the material's phase formation and crystallinity are affected by the solvent selection; well-optimized solvent systems improve phase purity and lessen the production of undesirable byproducts. The NCM523 cathode materials have been significantly affected by calcination temperature, which determines phase formation, crystallinity, and shape [25,26]. The excessive heat can cause agglomeration and phase transitions, which jeopardize the stability and transport of lithium ions, while the ideal temperatures maximize electrochemical performance.

The development of high-performance NCM523 cathodes that provide elevated battery efficiency relies on this fine-tuning. It is hypothesized that the introduction of EA and EG for the preparation of NCM523 cathode materials would provide a clean, affordable, environmentally friendly, thermally stable, and high-

View Article Online
DOI: 10.1039/D5NA00957J

purity material with improved crystallinity and electrochemical performance. Yet, to the best of our knowledge, the combined use of EG, water, and EA as a mixed solvent system for the synthesis of NCM523 has not been reported. To satisfy the above hypothesis, in this investigation, an alternative facile EG, water, and EA mediated mixed solvothermal method has been used to create NCM523 cathode materials and examine how various calcination temperatures affect the end products.

Materials and methods

Materials

All the chemicals were used as supplied, and no additional purification was carried out. Nickel acetate tetrahydrate ($Ni(CH_3COO)_2{\cdot}4H_2O$, 99%), cobalt acetate tetrahydrate ($Co(CH_3COO)_2{\cdot}4H_2O$ 98%), manganese acetate tetrahydrate ($Mn(CH_3COO)_2{\cdot}4H2O$, 99%), urea (NH_2-CO-NH_2, 99%), lithium carbonate (Li_2CO_3, 99%), and absolute ethanol were purchased from Sigma-Aldrich, Germany. Ethylene glycol (99.0%) and ethanolamine ($HOCH_2CH_2NH_2$, 99%) were collected from Qualikems, India, and Giant Chem Solution, USA, respectively. Deionized (DI) reverse osmosis and ultraviolet light were used to get water from Pureit (Taiwan).

Experimental

Stoichiometric ratios of $Ni(CH_3COO)_2{\cdot}4H_2O$, $Co(CH_3COO)_2{\cdot}4H_2O$, and $Mn(CH_3COO)_2{\cdot}4H_2O$ (molar ratio was 5:2:3) were dissolved in a mixture of ethylene glycol, deionized water, and ethanolamine of 80 mL (volume ratio was 0.5:0.25:0.25). The initial pH of the solution was 10.5±0.2, which ensured the steady hydrolysis. Under vigorous magnetic stirring, a specific quantity of urea (4.5 mmol) was added to the mixture as the chelating and slow-release precipitating agent until all the precursor salts dissolved completely. For comparison, identical stoichiometric ratios of metal acetate salts were separately dissolved in an EG/deionized water mixture (volume ratio 0.5:0.5) and pure EG solvent (80 mL). After that, the mixture

View Article Online
DOI: 10.1039/D5NA00957J

was placed in a 100 mL Teflon-lined stainless-steel autoclave (the filling capacity is fixed at around 80%), placed in a heating oven, and heated to 160 °C for 20 hours in order to produce the carbonate precursor. After the mixed solvothermal reaction, the precipitated product was cooled naturally to room temperature, centrifuged at 5000 rpm, washed three times with deionized water and ethanol each, and dried at 55 °C in a vacuum oven for 24 h. The as-obtained carbonate precursor was powdered, and an appropriate amount of Li_2CO_3 was mixed (lithium carbonate to precursor molar ratio =1.05:1) thoroughly in the agate mortar, and the obtained final precursor was annealed at 450 °C for 5h in the muffle furnace. Once the precursor mixture had naturally cooled to ambient temperature, it was equally ground once again and finally calcined at a certain temperature (700 °C, 800 °C, and 900 °C) for 12 h in the presence of air with a ramp rate of 20 °C/min. The NCM523 cathode materials were allowed to cool to room temperature and ground with 5 mm stainless steel balls in a 10:1 ball-to-powder ratio in a planetary ball mill (Pulverisetter 23, FRITSCH, Germany) at 50 Hz for 5 min with 15 balls (total 3.15 g). The typical solid-state product yield was 37-40.5%, depending on the solvent system and calcination temperature. The resulting powder was then collected and stored in an airtight container for characterization and fabrication of the electrode. The cathode materials were denoted as NCM7, NCM8, and NCM9 according to the calcination temperature of 700 °C, 800 °C, and 900 °C, respectively.

Materials characterization

The surface structure and particle size distributions of the prepared NCM523 cathode ingredients were analyzed by using a field-emission scanning electron microscope (FE-SEM, JEOL-7610F, Japan), operated at 15 kV, followed by ImageJ-based statistical analysis over 100-150 particles to ensure accurate morphology and size quantification. EDX spectra were taken with an energy-dispersive X-ray spectroscopy adaptor coupled to the FE-SEM instrument (JEOL-JED2300 Analysis station, Japan) operated at 15 kV. The surface elemental composition was investigated by X-ray photoelectron spectroscopy, XPS (XPS, K-alpha,

View Article Online
DOI: 10.1039/D5NA00957J

Thermo ScientificTM, USA). X-ray diffraction, (XRD, Panalytical, EMP3, Netherlands) patterns of the powder samples were used to determine the crystalline size and sample constituents.

Results and discussion

The impact of organic solvent composition on the crystallite size and phase purity of synthesized NCM523 cathode materials is clearly demonstrated by the XRD results, as shown in **Figure 1**. The diffraction patterns of all three cathode materials in three different solvent mixtures show peaks at two theta values of 18.93, 36.60, 37.57, 38.02, 44.40, 48.65, 59.70, 64.38, 64.78, and 68.19 corresponding to the lattice planes of 003, 101, 006, 102, 104, 105, 107, 108, 110, and 113, respectively. All of these patterns are accurately resemble to the combined identical phases of the cubic structure with space group Fd-3m of $Li_2CoMn_3O_8$ (JCPDS No. 48-0261), the rhombohedral (hexagonal axes) with space group R-3m of $LiNiO_2$ (JCPDS No. 09-0063), and the monoclinic crystal system with space group C2/c of $Li_{1.33}Mn_{0.67}O_2$ (JCPDS No. 27-1252) [23]. When EG alone was used as the reaction medium, the diffraction pattern (**Figure 1a**) displayed relatively broad and less intense peaks, together with several minor secondary reflections. Such features are typically associated with smaller crystallite size, incomplete crystallization, and the presence of undesirable impurity phases such as spinel or rock salt-type oxides. The poor crystallinity can be attributed to the fact that, while serving as both solvent and mild reducing agent, it provides limited hydrolysis capability and insufficient control over metal ion distribution. Consequently, the nucleation process occurs rapidly and homogeneously, leading to increased cation mixing, structural disorder, and suppressed long-range ordering in the layered lattice. The addition of water to EG produced a notable improvement in crystallinity and phase purity (**Figure 1b**). The XRD peaks became sharper and more intense, while the background noise and impurity reflections were significantly reduced. This enhancement can be rationalized by the role of water in promoting hydrolysis and increasing ionic

View Article Online
DOI: 10.1039/D5NA00957J

mobility, which results in more uniform mixing of Ni, Co, and Mn ions within the precursor solution [23]. A more homogeneous precursor composition facilitates a more controlled nucleation process during subsequent heat treatment, thereby yielding larger crystallites with reduced defect concentrations. This observation highlights the synergistic role of water in complementing EG by enhancing the solvation and reactivity of the metal ions. The best structural characteristics, however, were achieved when EA was introduced into the EG-water solvent system (**Figure 1c**). The XRD pattern of this sample showed the sharpest reflections with well-resolved splitting of the (006)/(102) and (018)/(110) doublets, which is the most reliable indicator of the formation of a highly ordered layered Fd-3m structure [27]. EA provides multiple benefits by strongly chelating transition metal ions to prevent premature precipitation, simultaneously acting as a pH buffer to stabilize the reaction medium and moderate hydrolysis rates, while also retarding nucleation kinetics to facilitate uniform and controlled crystal growth. These effects collectively suppress cation disorder, particularly the migration of Ni^{2+} into Li^{+} sites, and eliminate residual impurity phases. The superior ordering obtained in the EG, water, and EA system suggests reduced Li^{+}/Ni^{2+} cation mixing, which is crucial for ensuring high lithium-ion mobility and electrochemical performance. The degree of cation ordering in the prepared NCM523 samples was assessed via the intensity ratio of the (003) and (104) diffraction peaks, which serves as a consistent indicator of Ni^{2+}/Li^{+} cation mixing. The NCM523 synthesized using the EG-only one solvent system displayed an intensity ratio of 1.23, signifying a moderately ordered layered structure. The two-solvent system (EG+H_2O) exhibited a little lower ratio of 1.10, representing comparatively higher cation mixing and abridged structural ordering. In contrast, the three-solvent system (EG+H_2O+EA) generated a significantly higher ratio of 1.42, which surpasses the commonly acknowledged threshold (1.2) for well-ordered R-3m type layered oxides. Therefore, the three-solvent combination route demonstrates superior structural optimization and is the most appropriate solvent atmosphere for reaching high-quality NCM523 cathode materials.

View Article Online
DOI: 10.1039/D5NA00957J

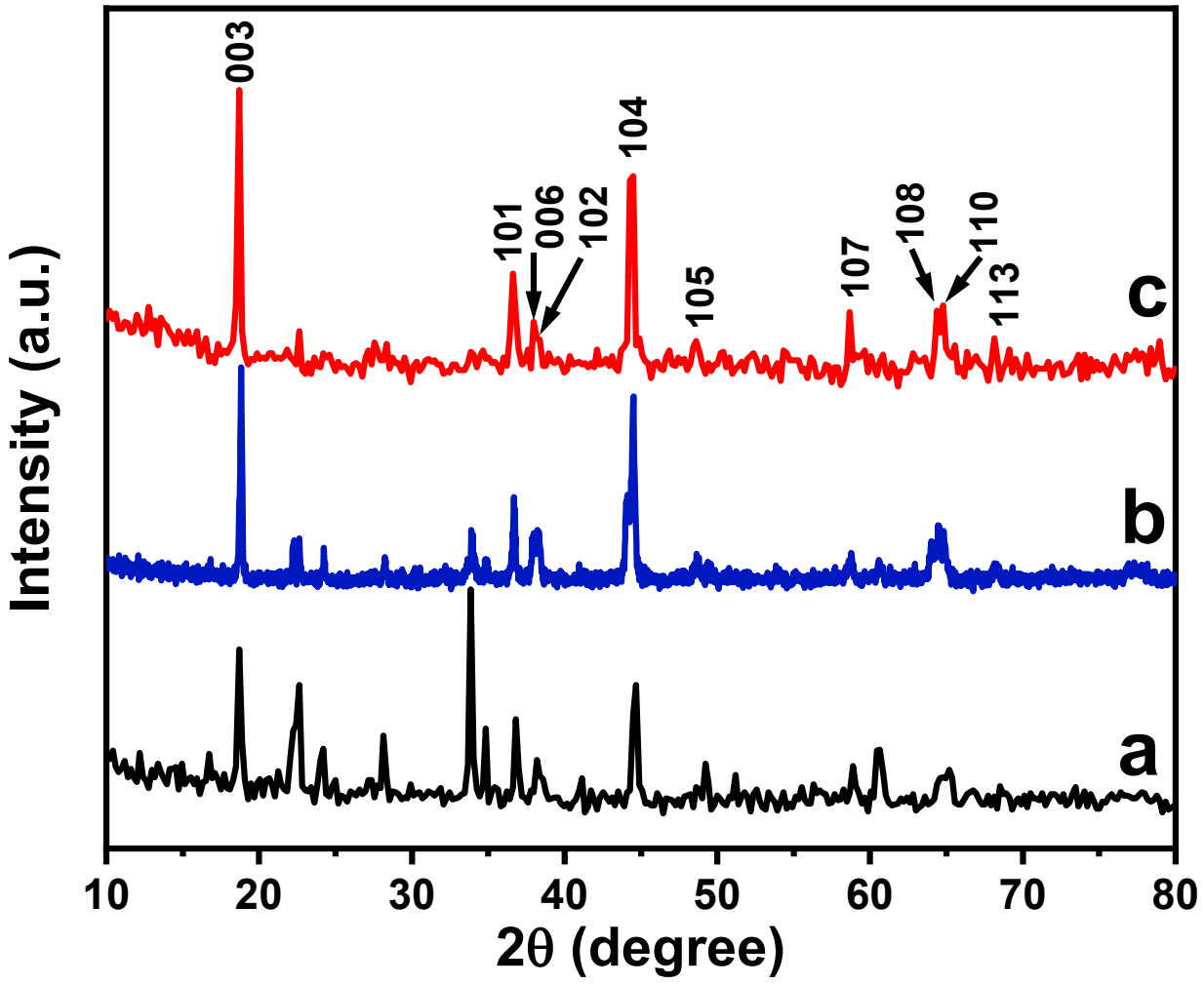

Figure 1. XRD diffraction patterns of NCM523 cathode materials synthesized using three solvent environments of a) EG, b) EG and water, and c) EG, water, and EA.

FTIR investigation reveals that the solvent environment strongly impacts the removal of residual functional groups and the formation of the metal-oxygen lattice (**Figure 2**). The precursor of NCM523 cathode materials, synthesized only in EG, shows strong O-H stretching (at around 3400 cm^{-1}) and bending (at around 1620 cm^{-1}) bands. This precursor also gives a robust C-O stretching band at 1130 cm^{-1} and bending vibrational mode at 865 cm^{-1}, along with a weak metal oxygen (M-O) vibrational mode arising from Ni, Co, and Mn within the layered oxide lattice in the region of 520-650 cm^{-1}, indicating unfinished decomposition[28]. Adding water to EG significantly decreases hydroxyl intensity and improves M-O

View Article Online
DOI: 10.1039/D5NA00957J

vibrations due to enhanced metal-ion hydrolysis. However, the three solvent system (EG+H_2O+EA) offers the cleanest FTIR profile, showing strongly suppressed O-H and C-O vibrations and the sharpest M-O vibrational bands, confirming superior precursor homogeneity and more efficient metal-ligand coordination. Therefore, the three solvent-derived (EG+H_2O+EA) precursor was selected as the most reliable synthesis pathway, and all subsequent stages of this study, including calcination at three different temperatures and comprehensive structural and morphological characterizations, were carried out using this optimized material.

Table 1. Effect of solvent environment on NCM523 cathode materials.

Sample condition	**O-H vibrations (3400 & 1620 cm^{-1})**	**C-O vibrations (1130 & 865 cm^{-1})**	**M-O bands (520-650 cm^{-1})**	**Interpretation**
EG	Strong	Strong	Weak	Poor precursor decomposition, disordered network
EG+H_2O	Moderate	Reduced	Improved	Better hydrolysis and coordination
EG+H_2O+EA	Lowest	Strongly suppressed	Strongest & sharpest	Highly uniform precursor, best structural development

View Article Online
DOI: 10.1039/D5NA00957J

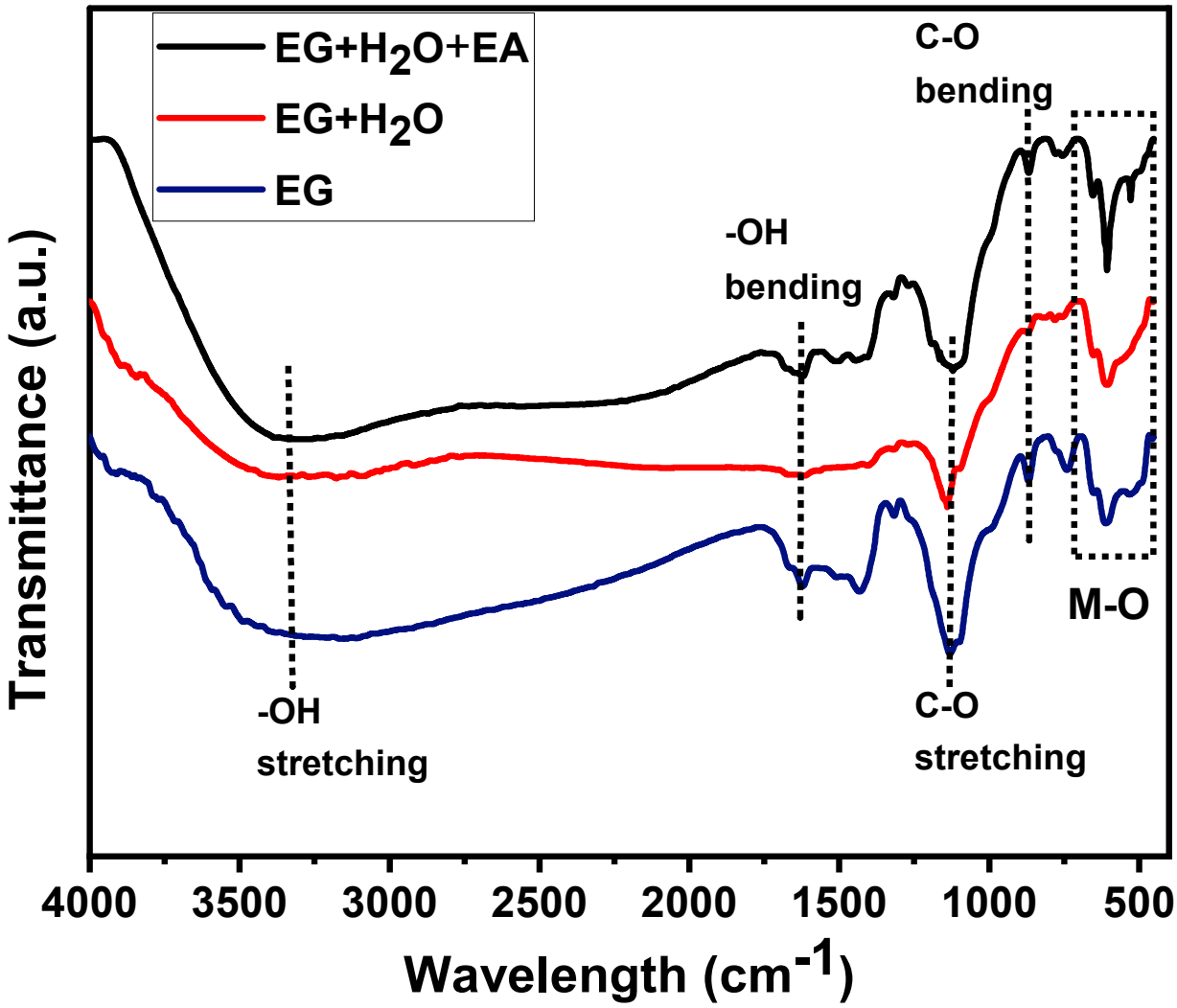

Figure 2. FTIR spectra of NCM523 cathode materials synthesized using three solvent environments.

The thermal decomposition behavior of the NCM523 carbonate precursor was estimated by TGA, and the resulting curve displays three distinct mass-loss regions characteristic of solvothermally derived mixed-metal carbonates (**Figure 3**). The first minor weight loss below 200 °C resembles the evaporation of physically adsorbed moisture and residual solvent molecules from the precursor surface. A more noticeable mass loss is observed between 200-450 °C, which is attributed to the decomposition of organic species originating from the solvothermal medium and the partial breakdown of metal-carbonate

View Article Online
DOI: 10.1039/D5NA00957J

intermediates. A major decomposition step occurs between 500-750 °C, connected with the complete decarboxylation of lithium carbonate and the formation of Co, Ni, Mn, and Li oxides phases[29]. Beyond 800 °C, the TGA curve reaches a stable plateau, displaying no additional mass loss. This thermal stability region confirms the selection of 800 °C as the final calcination temperature, ensuring full conversion to the layered oxide structure without further decomposition. Overall, the TGA profile supports the chosen thermal treatment route and confirms the precursor's complete transformation into a stable oxide phase at elevated temperatures.

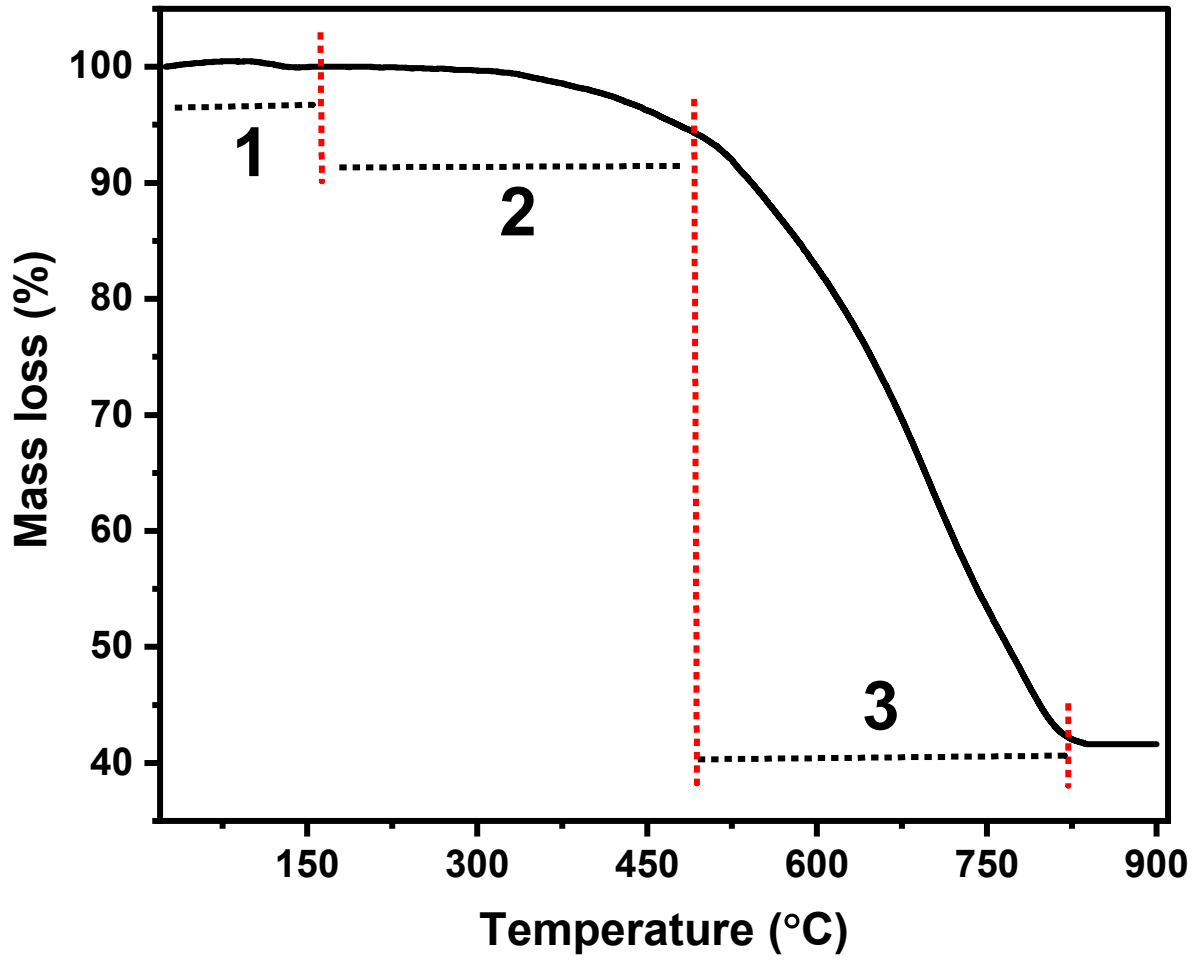

Figure 3. TGA thermographs of NCM523 precursor.

View Article Online
DOI: 10.1039/D5NA00957J

The impact of different calcination temperatures on the crystallite size and phase purity of synthesized NCM523 cathode materials is analyzed using XRD diffraction patterns and is shown in **Figure 4**. The intensity ratios of the diffraction patterns of 003/104 planes and the degree of the peak splitting of 006/102 and 108/110 are a good indication of layered structure materials [27,30]. The NCM-800 diffraction peaks display the best layered structure with no discernible impurity reflections, and the creation of a typical layered structure is indicated by the obvious full splitting of the pair reflections of (006)/(102) and (108)/(110) (**Figure 4b**). Since this displacement (Ni^{2+} at 3a site and Li^{+} at 3b site in the space group of layered R-3m) weakens the intensity of the (003) line without changing the intensity of the (104) peaks, the integrated intensity ratio of the (003) and (104) peaks is often employed to define the Li^{+}/Ni^{2+} cation mixing [31]. When the ratio is higher (>1.2), the degree of cation mixing is lower. We can find out that NCM-800 has a higher concentration value of 1.42 compared to the NCM-700 cathode materials (1.29) (**Figure 4a**). At high calcination temperature (**Figure 4c**), the intensity of the diffraction peak of the (003) plane significantly reduces to a minimum value compared to NCM-700 and NCM-800 cathode materials.The intensity ratio decreases to 0.76 because excessive calcination temperature causes structural degradation and increases cation mixing in NCM523 cathode materials. Compared to NCM-700, which shows broader XRD peaks indicative of poor crystallinity and possible structural defects, NCM-800 demonstrates sharper peaks, suggesting improved phase purity and reduced cation mixing. The crystallite size of the NCM523 samples varied noticeably with calcination temperature. At 700 °C, the crystallite size was 31 nm, demonstrating the primary growth of the layered structure. Increasing the temperature to 800 °C enhanced crystal growth, creating the largest crystallite size of 37 nm, which reflects improved crystallinity. However, further heating to 900 °C reduced the crystallite size to 26 nm, signifying structural instability and the onset of thermal degradation at excessively high temperatures.

View Article Online
DOI: 10.1039/D5NA00957J

32

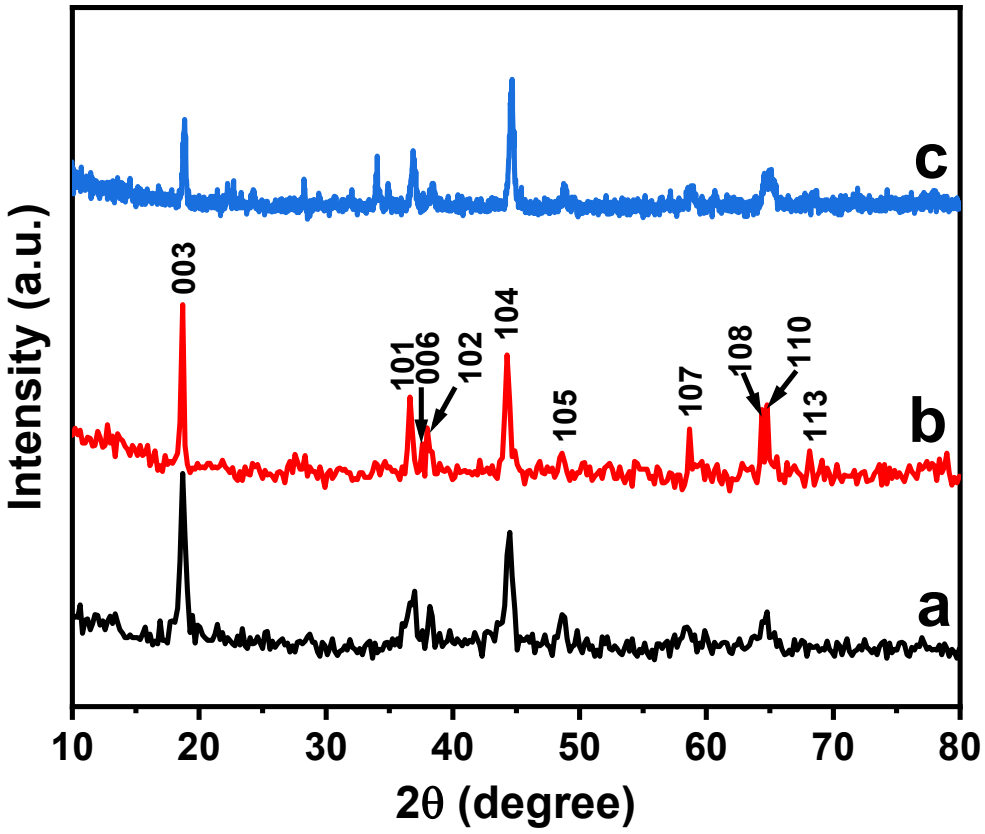

Figure 4. XRD diffraction patterns of NCM523 cathode materials calcined at (a) 700 °C, (b) 800 °C, and (c) 900 °C.

The Rietveld refinement of the NCM523 cathode materials calcined at 800 °C is shown in **Figure 5,** and the values of lattice parameters for XRD patterns are calculated and summarized in **Table 2**. The analysis reveals well-defined lattice parameters of a=2.8755 Å and c=14.1806 Å, giving a c/a ratio of 4.9315, which is characteristic of a well-ordered R-3m layered structure. A higher c/a ratio usually indicates better separation between the lithium and transition-metal layers and agrees with lower Li/Ni interlayer mixing[33]. This is consistent with the refined cation occupancy, which displays only 0.022 Ni present on the Li (3a) site, corresponding to a Li/Ni mixing level of around 2.2%. Such a low mixing percentage authorizes

View Article Online
DOI: 10.1039/D5NA00957J

that the 800 °C sample keeps strong structural ordering, negligible cation disorder, and even layer stacking properties that typically boost lithium-ion diffusion and electrochemical performance.

Table 2: Lattice parameter of NCM8 sample

SAMPLE	LATTICE PARAMETER			I(003)/I(104)	Li^{+}/Ni^{2+} MIXING
	a(Å)	c(Å)	c/a		(%)
NCM8	2.8755	14.1806	4.9315	1.42	2.2

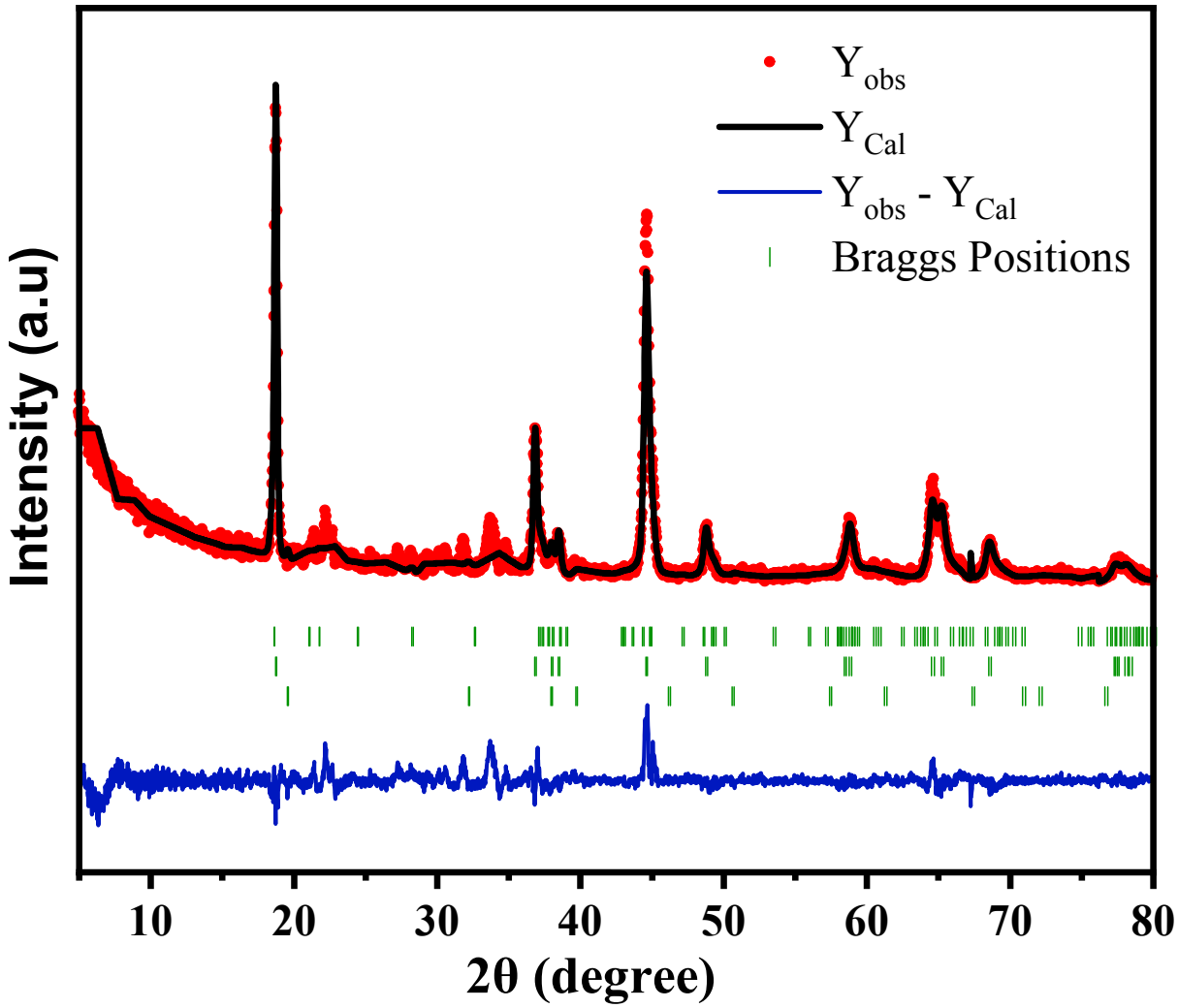

Figure 5. Rietveld refinement results of NCM523 cathode materials calcined at 800 °C.

View Article Online
DOI: 10.1039/D5NA00957J

A comparative FTIR spectra of the 700, 800, and 900 °C calcined samples display a significant influence of temperature on their purity and are shown in **Figure 6**. The NCM7 exhibits strong O-H stretching (at approximately 3400 cm^{-1}) and bending (at approximately 1620 cm^{-1}) bands, along with pronounced C-O vibrations, indicating incomplete decomposition of hydroxyl and organic species. At 800 °C, these peaks are significantly reduced, and the M-O stretching region of 520-650 cm^{-1} becomes sharper and more powerful, demonstrating enhanced crystallization and development of the layered NCM523 structure. Although the 900 °C precursor shows minimal organic signals, the M-O bands become broadened, signifying lattice distortion/defect generation at excessively high temperatures. These verdicts approve that 800 °C is the most favorable calcination temperature, providing the best balance between organic removal and structural ordering.

Table 3. Effect of calcination temperature on NCM523 cathode materials.

CALCINATION TEMPERATURE	**O-H VIBRATIONS (3400 & 1620 CM^{-1})**	**C-O VIBRATIONS (1130 & 865 CM^{-1})**	**M-O BANDS (520-650 CM^{-1})**	**INTERPRETATION**
700 °C	Strong	Strong	Weak/broad	Incomplete decomposition, low structural order
800 °C	Reduced	Suppressed	Strong/sharp	Optimal layered oxide formation
900 °C	Minimal	Very weak	Broadened	Over calcination, lattice distortion

View Article Online
DOI: 10.1039/D5NA00957J

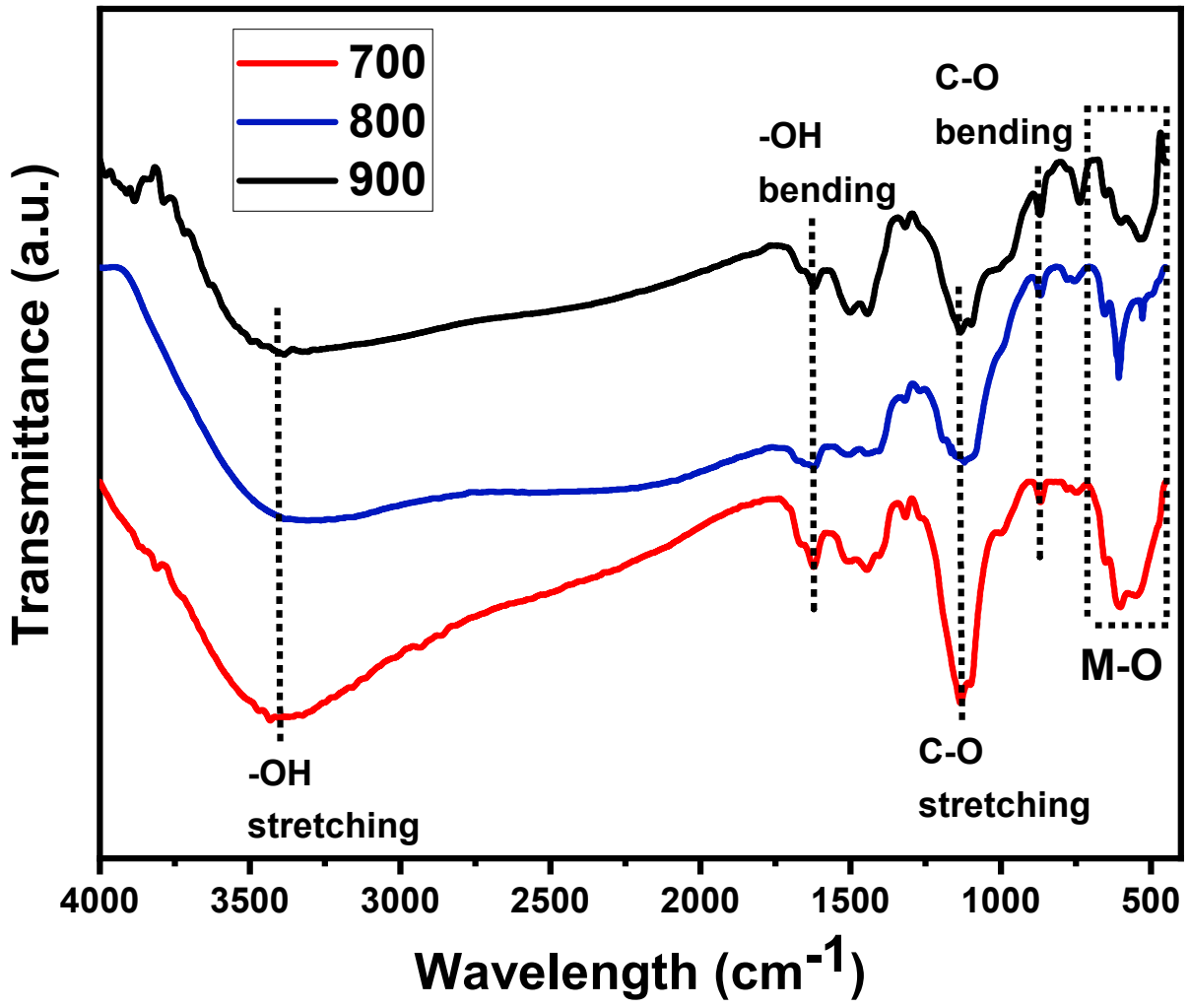

Figure 6. FTIR spectra of NCM52 cathode materials at different calcination temperatures 700 (red line), 800 (blue line), and 900 ˚C (black line).

The elemental composition and the variation of the oxidation state of each transition metal ion in the NCM523 cathode materials are detected by XPS spectra and are illustrated in **Figure 7**. The survey spectra (**Figure 7a**) of each cathode material show the spectra of the Li1s, C1s, O1s, Mn2p, Co2p, and Ni2p without any impurities. The O 1s spectra of the NCM523 cathode materials are deconvoluted into three peaks that reflect distinct oxygen atmospheres within the material (**Figure 7b**). The low binding energy peak at 529.2

View Article Online
DOI: 10.1039/D5NA00957J

eV resembles O^{2-} ions bonded to transition metals, representing stable lattice oxygen in the layered structure. The high binding energy peak at 531.4 eV originates from surface species of -CO_3, adsorbed H_2O, and -OH groups. The intermediate peak (530.35 eV) from oxygen is involved in defect-rich regions, including vacancy-related O^{2-} or partially hydroxylated sites[34]. The spectrum also highlights that NCM-800 has the highest $O_{lattice}/O_{surface}$ ratio of 0.26, suggesting minimal oxygen vacancies and a well-developed metal oxygen framework. In contrast, the NCM7 sample displays a much lower ratio (0.13), reflecting partial oxidation and the existence of surface-bound hydroxyls and carbonates due to insufficient thermal decomposition. The 900 °C sample also demonstrates a reduced ratio (0.11), which is attributed to excessive oxygen loss and defect generation at high temperature. The Li1s spectrum of NCM-800 presents a sharp and well-defined peak at a binding energy of 58.5 eV, confirming effective lithium incorporation, unlike NCM-700, which has a weaker Li signal, or NCM-900, which shows signs of lithium loss [22] (**Figure 7c**). The XPS spectra of Co2p (**Figure 7d**) consist of two main points of $Co2p_{3/2}$ (~780 eV) and $Co2p_{1/2}$ (~795 eV), along with corresponding satellite peaks at higher binding energies [22]. The 800 °C sample displays a Co^{2+}/Co^{3+} ratio of 0.24, indicating a dominant presence of Co^{3+}, which is characteristic of a well-formed layered structure with steady transition metal oxidation states. In comparison, the 700 °C sample shows a higher ratio (0.37), suggesting incomplete oxidation and a higher fraction of Co^{2+} associated with residual defects, hydroxyl groups. The 900 °C sample also presents an elevated ratio (0.31), which is typically associated with thermal over-reduction and increased surface defect formation. The peak position of Ni2p in **Figure 7e** of all three cathode materials shows doublet characteristics lines with the binding energy standards positioned at 854.6 eV and 873.5 eV, assignable to $Ni2p_{3/2}$ and $Ni2p_{1/2}$, respectively. The variation in binding energy between the $Ni2p_{3/2}$ and $Ni2p_{1/2}$ is ~18.9 is well agreed with the standard references of Ni^{2+} cations [35]. The intensity of $Ni2p_{3/2}$ and $Ni2p_{1/2}$ lines was relatively high for NCM-800 cathode materials compared to the other two cathode materials, while it was minimal for the NCM-900 sample. Less noticeable peaks in the NCM-900 cathode material are seen at 856.0 and 874.5

View Article Online
DOI: 10.1039/D5NA00957J

eV, suggesting the existence of trace amounts of Ni^{3+} cation. A satellite peak around 861.9 eV was observed between the $Ni2p_{3/2}$ and $Ni2p_{1/2}$ regions, caused by the splitting of energy levels in nickel oxides. This splitting occurs due to the interaction of core electrons with the surrounding electron cloud in the nickel oxide structure, leading to a shift in binding energy [33]. The 800 °C sample displays a Ni^{2+}/Ni^{3+} ratio of 0.23, indicating efficient oxidation of Ni^{2+} to Ni^{3+} and a well-stabilized layered structure with limited cation disorder. In contrast, the 700 °C sample shows a noticeably lower ratio of 0.15, suggesting incomplete oxidation. The 900 °C sample, however, shows a markedly increased ratio of 0.89, which points toward thermal over-reduction and oxygen deficiency at elevated temperatures. Such a high Ni^{2+} content typically leads to increased Li^{+}/Ni^{2+} mixing and structural degradation. The Mn2p spectrum of NCM-800 reflects the electron binding energy at 642.5 eV and 638.8 eV for Mn 2p3/2, which indicates the existence of both Mn^{2+} and Mn^{4+} ions [33,36]. The presence of both Mn^{2+} and Mn^{4+} ions contributes to phase stability, while NCM-700 exhibits some Mn^{4+}, which can lead to structural degradation. The 800 °C sample exhibits a Mn^{2+}/Mn^{4+} ratio of 0.52, representing a favorable distribution dominated by the electrochemically active Mn^{4+} state, which supports structural stability and suppresses Jahn-Teller distortions. At 700 °C, the ratio drops to 0.17, indicative of incomplete oxidation and a higher proportion of Mn^{2+} caused by insufficient thermal energy. Meanwhile, the 900 °C sample shows a ratio of 0.39, reflecting partial over-reduction and oxygen loss at excessively high temperatures.

Table 4. Summary of compositional and $O_{lattice}/O_{surface}$ ratios obtained from XPS analysis.

SAMPLE	NI^{2+}/NI^{3+}	CO^{2+}/CO^{3+}	MN^{2+}/MN^{4+}	$O_{LATTICE}/O_{SURFACE}$
700 °C	0.15	0.37	0.17	0.13
800 °C	0.23	0.24	0.52	0.26
900 °C	0.89	0.31	0.39	0.11

View Article Online
DOI: 10.1039/D5NA00957J

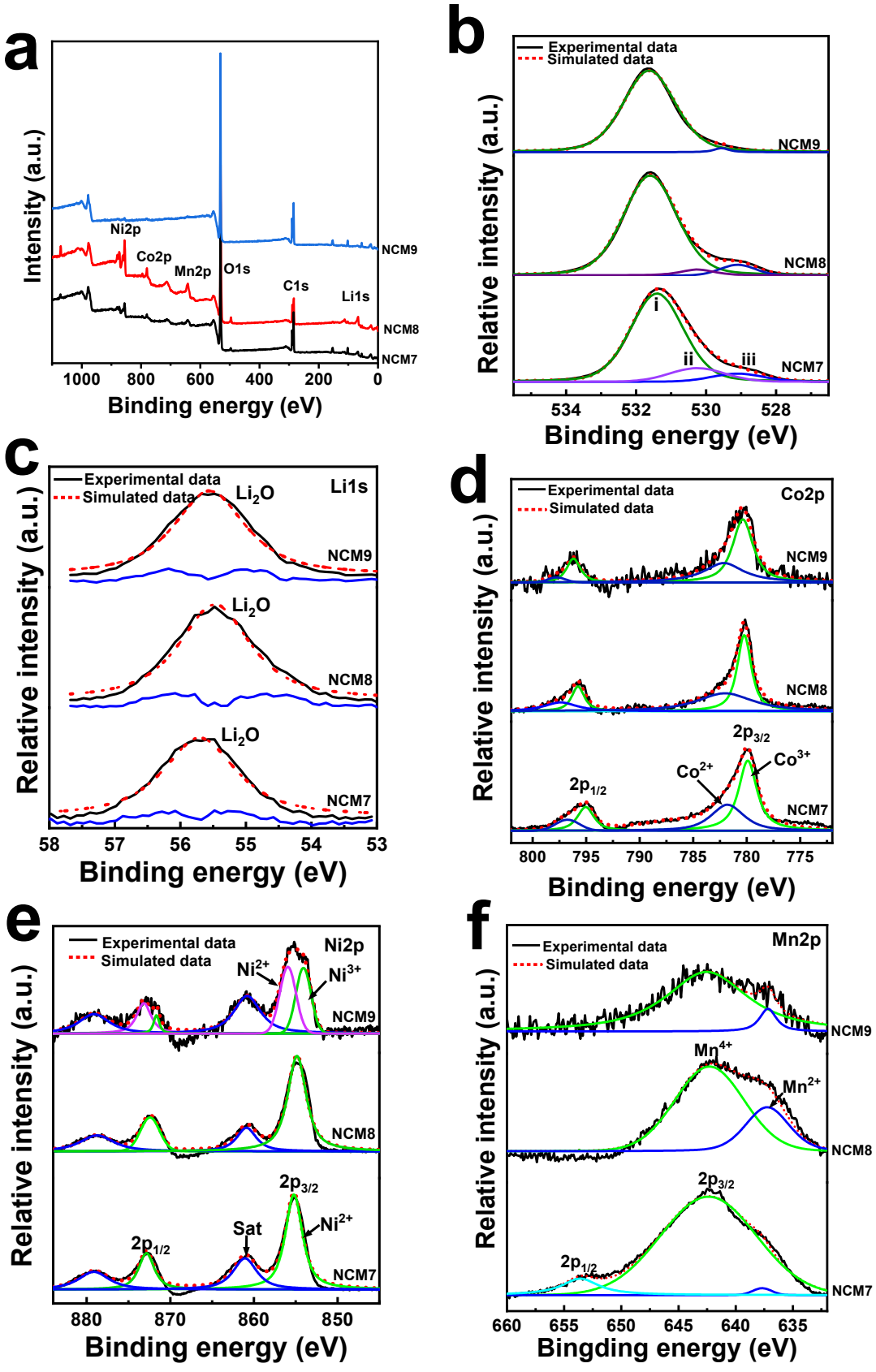

View Article Online
DOI: 10.1039/D5NA00957J

Figure 7. X-ray photoelectron spectroscopy of (a) survey spectrum and deconvoluted core line spectra of (b) O1s, (c) Li1s, (d) Co2p, (e) Ni2p, and (f) Mn2p of NCM523 cathode materials, where NCM7, NCM8, and NCM9 indicate the calcined temperature of 700 °C, 800 °C, and 900 °C, respectively.

The particle morphology, size distribution, and structural integrity of the surfaces of NCM523 cathode materials calcined at different temperatures of 700°C, 800°C, and 900°C were examined using FE-SEM and are shown in **Figure 8**. The NCM523 cathode materials calcined at 700 °C are composed of small, loosely packed nanoparticles, and then these primary nanoparticles aggregate to form secondary particles with significant porosity, incomplete crystallization, and an irregular shape (**Figure 8a and 8b**). At 800°C, the NCM523 particles exhibit more uniform spherical secondary particles composed of tightly packed primary nanoparticles, with smooth surfaces and minimal cracks, indicating optimal crystallinity and agglomeration for balanced electrochemical performance. In contrast to NCM-800, excessive sintering at 900°C results in larger, fused particles with microcracks and inhomogeneous grain growth, which degrade cycling stability and may exacerbate mechanical stress during charge/discharge (**Figure 8e and 8f**). At 900°C, particle size distributions become much wider, but at 800°C, they maintain a small, Gaussian-like distribution perfect for long-term use and high tap density. These results are consistent with previous research, indicating that 800°C is the ideal calcination temperature for NCM523, striking a balance between particle uniformity, structural integrity, and electrochemical efficiency [37]

View Article Online
DOI: 10.1039/D5NA00957J

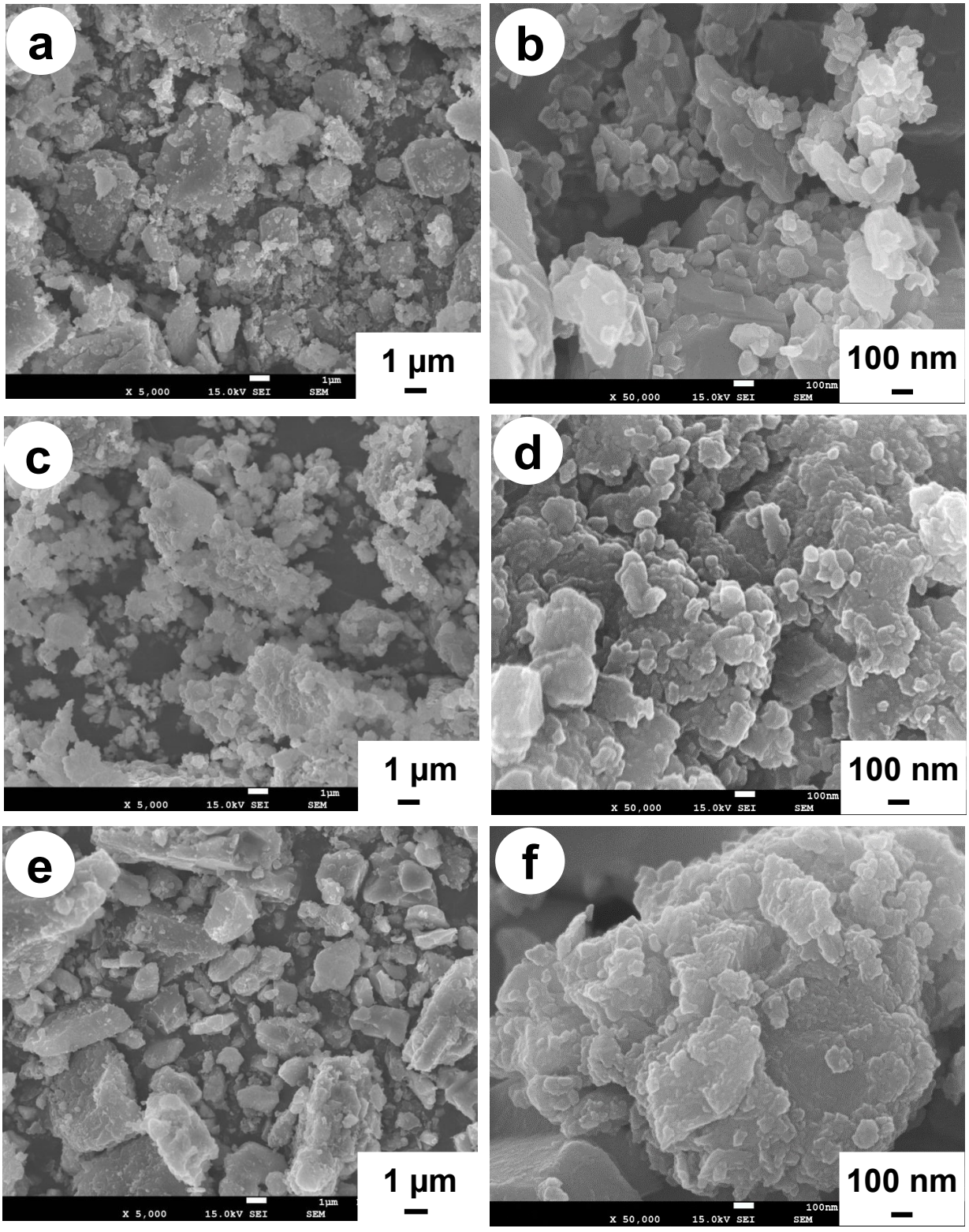

View Article Online
DOI: 10.1039/D5NA00957J

Figure 8. FE-SEM images of NCM523 cathode materials at different magnification values (5K and 50K) calcined at (a, b) 700 °C, (c, d) 800 °C, and (g, h) 900 °C respectively.

The EDS analysis of NCM523 cathode materials calcined at 700°C, 800°C, and 900°C provides crucial insights into elemental composition and distribution. The spectrum of the 700°C sample (**Figure 9 a**) confirms the presence of Ni, Co, Mn, and O, but with signs of inhomogeneous distribution and possible residual Li_2CO_3 or LiOH, indicating incomplete crystallization. This cathode materials also exhibit deviation from the 5:2:3 stoichiometry (Ni≈48.2%, Co≈18.5%, Mn≈33.3%) with Mn surface segregation and residual Li_2CO_3 (C≈5.2%, O≈57%), indicating incomplete calcination, leading to poor cation diffusion. This suggests that the material may have phase impurities and an imbalanced Ni:Co:Mn ratio, which could negatively impact electrochemical performance. In contrast, the 800°C sample (**Figure 9 b**) exhibits a highly uniform element distribution with near-ideal ratios (Ni≈49.8%, Co≈20.1%, Mn≈30.1%) with homogeneous cation distribution and minimal carbon (C≈0.8%), ensuring structural integrity and the best balance of elements. However, the 900 °C sample (**Figure 9 c**) shows Ni depletion (≈44.7%) and Mn enrichment (≈33.5%) due to thermal-driven cation migration, resulting in Mn-rich grain boundaries and trace Ni reduction (≈5.1%) in the final composition, promoting Mn^{3+} Jahn-Teller distortion and oxygen loss. This may lead to structural degradation, elemental segregation, and cation migration, potentially reducing the cathode's long-term stability. Overall, the NCM-800 sample demonstrates the most favorable elemental distribution with minimal defects for high-performance NCM523 cathode materials[37].

View Article Online
DOI: 10.1039/D5NA00957J

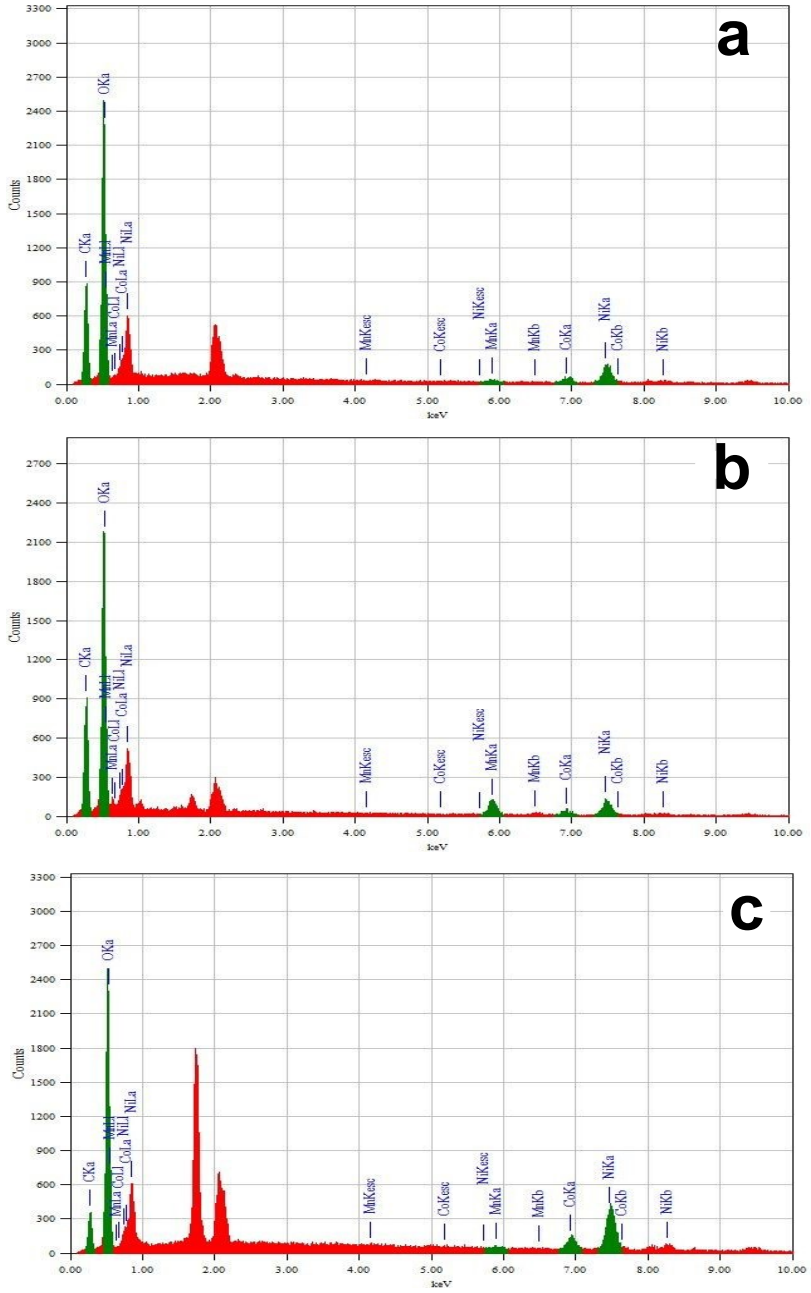

Figure 9. EDS spectra of NCM523 cathode materials calcined at (a) 700 °C, (b) 800 °C, and (c) 900 °C

The TEM micrographs of the NCM523 sample calcined at 800 °C (**Figure 10**) reveal well-developed primary particles and a highly crystalline layered structure. The low-magnification image (**Figure 10a**) shows that

View Article Online
DOI: 10.1039/D5NA00957J

the secondary particles recall an aggregated morphology with particle clusters in the sub-micron to micron range, which is characteristic of well-sintered layered oxide cathodes. The intermediate magnification TEM image (**Figure 10b**) displays loosely packed primary nanoparticles with sizes typically below 200 nm. High-resolution TEM (**Figure 10c**) confirms the formation of a well-ordered layered structure, as demonstrated by clear lattice fringes corresponding to the (003) plane with an interplanar spacing of d003=0.47 nm, which agrees well with the characteristic spacing of the trigonal R-3m NCM523 cathode materials[22]. The sharp and continuous lattice fringes also indicate low structural defects and high crystallinity, further supporting that calcination at 800 °C provides optimal ordering and phase purity for NCM523.

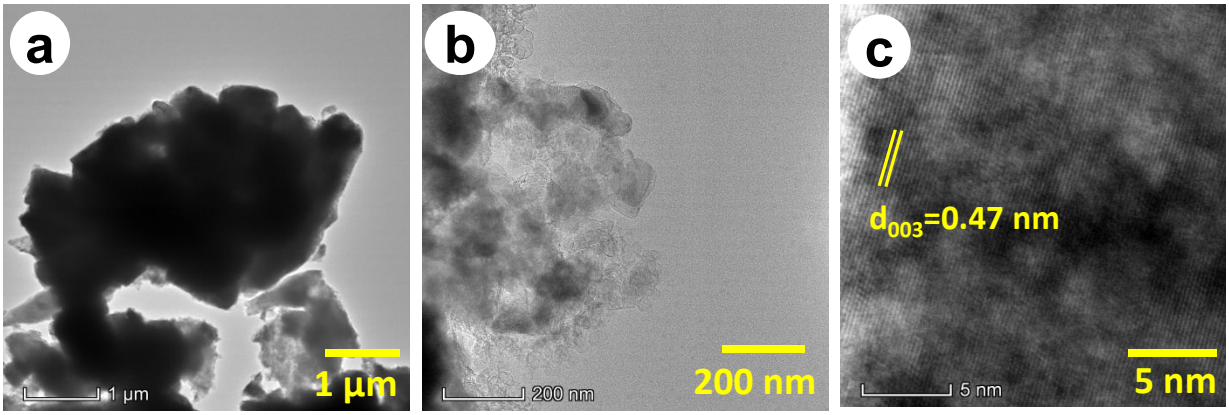

Figure 10. a) TEM images at low magnification, and b) High magnification, C) HRTEM images of NCM523 cathode material calcined at 800 °C.

Conclusion

In this investigation, particular emphasis is placed on developing a low-cost, environmentally friendly, thermally stable, and high-purity $LiNi_{0.5}Co_{0.2}Mn_{0.3}O_2$ (NCM523) cathode material. This work systematically demonstrates that both the solvent composition during precursor synthesis and the calcination

View Article Online
DOI: 10.1039/D5NA00957J

temperature play critical roles in defining the final quality of NCM523 cathode materials. Among the evaluated solvent systems, the combination of EG, water, and EA proved superior due to its durable metal chelating capability, improved hydrolysis control, and ability to control nucleation kinetics. This synergy produced a highly uniform precursor that exhibited excellent crystallinity, well-resolved layered structural features, and the highest (003)/(104) intensity ratio (1.42) among all NCM523 cathode materials. FTIR investigation further established that this solvent system minimizes residual organic species and promotes the development of a stable M-O lattice network. Upon calcination, the 800 °C sample confirmed the optimal balance of crystallite growth, cation ordering, and oxygen stability, as demonstrated by its favorable Ni^{2+}/Ni^{3+}, Co^{2+}/Co^{3+}, and Mn^{2+}/Mn^{4+} ratios. The $O_{lattice}/O_{surface}$ value ratio reaches 0.26, significantly higher than at 700 °C (0.13) and 900 °C (0.11), confirming improved lattice oxygen stability and fewer surface defects. In contrast, lower temperatures led to incomplete oxidation and structural immaturity, while higher temperatures caused oxygen loss and defect generation. Therefore, the integrated approach of three solvent-assisted precursor synthesis followed by calcination at 800 °C yields the most phase-pure, structurally ordered, and chemically stable NCM523 material. These findings provide a comprehensive pathway for optimizing synthesis parameters to achieve high-performance layered cathode materials suitable for demanding lithium-ion battery technologies.

Author Contributions

S.R.: data curation, formal analysis, investigation, validation, writing-original draft. A.R.: formal analysis, investigation, methodology, visualization, validation, writing-review & editing. R.H.: visualization. M.S.: investigation, validation. A.N.A.: formal analysis. M.S.Q.: formal analysis. C.K.R.: formal analysis. M.H.:

View Article Online
DOI: 10.1039/D5NA00957J

writing-review & editing. M.S.J.: conceptualization, funding acquisition, project administration, validation, supervision, writing–review &editing.

Conflicts of interest

The authors declare that they have no conflict of interest.

Acknowledgments

This research was conducted as part of the R&D project (FY 2025-2026) of IERD, BCSIR, called “Synthesis and optimization of $LiNi_{1-x-y}Co_xMn_yO_2$ for use as cathode materials in advanced energy storage devices.” We especially thank Shahran Ahmed Joy and Nadim, Munna, scientific officer, Institute of Mining, Mineralogy and Metallurgy (IMMM), BCSIR, Joypurhat, for their support on Rietvelt Refinement and TGA analysis.

View Article Online
DOI: 10.1039/D5NA00957J

References

1 H. Li, Y. Ren, P. Yang, Z. Jian, W. Wang, Y. Xing and S. Zhang, *Electrochim Acta*, 2019, **297**, 406–416.

2 D. Ma, Y. Li, P. Zhang, A. J. Cooper, A. M. Abdelkader, X. Ren and L. Deng, *J Power Sources*, 2016, **311**, 35–41.

3 H. Ding, X. Wang, J. Wang, H. Zhang, G. Liu, W. Yu, X. Dong and J. Wang, *J Power Sources*, 2023, **553**, 232307.

4 B. Qiu, C. Yin, Y. Xia and Z. Liu, *ACS Appl Mater Interfaces*, 2017, **9**, 3661–3666.

5 Z. Cui, F. Zou, H. Celio and A. Manthiram, *Adv Funct Mater*, DOI:10.1002/adfm.202203779.

6 B. Wu, H. Xu, D. Mu, L. Shi, B. Jiang, L. Gai, L. Wang, Q. Liu, L. Ben and F. Wu, *J Power Sources*, 2016, **304**, 181–188.

7 P. S. Maram, G. C. C. Costa and A. Navrotsky, *Angewandte Chemie International Edition*, 2013, **52**, 12139–12142.

8 M. Y. Song and R. Lee, *J Power Sources*, 2002, **111**, 97–103.

9 K. Vijaya Babu, L. Seeta Devi, V. Veeraiah and K. Anand, *Journal of Asian Ceramic Societies*, 2016, **4**, 269–276.

10 X. Zhu, F. Meng, Q. Zhang, L. Xue, H. Zhu, S. Lan, Q. Liu, J. Zhao, Y. Zhuang, Q. Guo, B. Liu, L. Gu, X. Lu, Y. Ren and H. Xia, *Nat Sustain*, 2020, **4**, 392–401.

11 Y. Hong, C. Li, J. Ouyang, Q. Hu, X. Wang, Z. Tang and T. Liu, *Scr Mater*, 2024, **241**, 115878.

12 Y. Zhang, Q. Huo, P. Du, L. Wang, A. Zhang, Y. Song, Y. Lv and G. Li, *Synth Met*, 2012, **162**, 1315–1326.

View Article Online
DOI: 10.1039/D5NA00957J

13 K. Ben-Kamel, N. Amdouni, A. Mauger and C. M. Julien, *J Alloys Compd*, 2012, **528**, 91–98.

14 Y. Li, Q. Han, X. Ming, M. Ren, L. Li, W. Ye, X. Zhang, H. Xu and L. Li, *Ceram Int*, 2014, **40**, 14933–14938.

15 W. Liu, X. Li, Y. Hao, D. Xiong, H. Shan, J. Wang, W. Xiao, H. Yang, H. Yang, L. Kou, Z. Tian, L. Shao and C. Zhang, *Adv Funct Mater*, DOI:10.1002/adfm.202008301.

16 C. Roitzheim, L.-Y. Kuo, Y. J. Sohn, M. Finsterbusch, S. Möller, D. Sebold, H. Valencia, M. Meledina, J. Mayer, U. Breuer, P. Kaghazchi, O. Guillon and D. Fattakhova-Rohlfing, *ACS Appl Energy Mater*, 2022, **5**, 524–538.

17 X. Dai, A. Zhou, J. Xu, B. Yang, L. Wang and J. Li, *J Power Sources*, 2015, **298**, 114–122.

18 S. Shi, T. Wang, M. Cao, J. Wang, M. Zhao and G. Yang, *ACS Appl Mater Interfaces*, 2016, **8**, 11476–11487.

19 J. Zheng, W. Zhou, Y. Ma, H. Jin and L. Guo, *J Alloys Compd*, 2015, **635**, 207–212.

20 M. Jiang, Q. Zhang, X. Wu, Z. Chen, D. L. Danilov, R.-A. Eichel and P. H. L. Notten, *ACS Appl Energy Mater*, 2020, **3**, 6583–6590.

21 X. Jiang, Y. Sha, R. Cai and Z. Shao, *J Mater Chem A Mater*, 2015, **3**, 10536–10544.

22 J. Fang, H. An, F. Qin, H. Wang, C. Chen, X. Wang, Y. Li, B. Hong and J. Li, *ACS Appl Mater Interfaces*, 2020, **12**, 55926–55935.

23 X. Hou, Y. Huang, S. Ma, X. Zou, S. Hu and Y. Wu, *Mater Res Bull*, 2015, **63**, 256–264.

24 Y. Liu, T. Moser, C. Andres, L. Gorjan, A. Remhof, F. Clemens, T. Graule, A. N. Tiwari and Y. E. Romanyuk, *J Mater Chem A Mater*, 2019, **7**, 3083–3089.

View Article Online
DOI: 10.1039/D5NA00957J

25 S. Dong, Y. Zhou, C. Hai, J. Zeng, Y. Sun, Y. Shen, X. Li, X. Ren, G. Qi and L. Ma, *Ionics (Kiel)*, 2019, **25**, 5655–5667.

26 W. Ahn, S. N. Lim, K.-N. Jung, S.-H. Yeon, K.-B. Kim, H. S. Song and K.-H. Shin, *J Alloys Compd*, 2014, **609**, 143–149.

27 Y. Sun, Y. Zhou, L. Zhang, Y. Shen and J. Zeng, *J Alloys Compd*, 2017, **723**, 1142–1149.

28 C. S. Yudha, S. U. Muzayanha, H. Widiyandari, F. Iskandar, W. Sutopo and A. Purwanto, *Energies (Basel)*, DOI:10.3390/en12101886.

29 J. P. Yasnó, S. Conconi, A. Visintin and G. Suárez, *J Anal Sci Technol*, DOI:10.1186/s40543-021-00267-5.

30 F. Wu, M. Wang, Y. Su, L. Bao and S. Chen, *J Power Sources*, 2010, **195**, 2362–2367.

31 J. Zhu, J. Zheng, G. Cao, Y. Li, Y. Zhou, S. Deng and C. Hai, *J Power Sources*, 2020, **464**, 228207.

32 J. Li, M. Zhang, D. Zhang, Y. Yan, Z. Li and Z. Nie, *Int J Electrochem Sci*, 2020, **15**, 1881–1892.

33 Y. Zhang, C. Cui, Y. He, J. Liu, Y. Song, Z. Song, H. Xu, S. Huang and Y. Bei, *Mater Chem Phys*, 2021, **262**, 124269.

34 A. Sharma, R. Abdur, D. Kim, A. K. Tripathi, S. Singh, J. Lee and S. I. Yoo, *Current Applied Physics*, 2020, **20**, 1041–1048.

35 M. Cheng, H. Fan, Y. Song, Y. Cui and R. Wang, *Dalton Trans.*, 2017, **46**, 9201–9209.

36 S. Dong, Y. Zhou, C. Hai, J. Zeng, Y. Sun, Y. Shen, X. Li, X. Ren, G. Qi and L. Ma, *Ionics (Kiel)*, 2019, **25**, 5655–5667.

37 W. Ahn, S. N. Lim, K.-N. Jung, S.-H. Yeon, K.-B. Kim, H. S. Song and K.-H. Shin, *J Alloys Compd*, 2014, **609**, 143–149.

View Article Online
DOI: 10.1039/D5NA00957J

Supporting data and the findings of this study are available from the corresponding author upon reasonable request.